(Received 19 March 2025, Accepted 15 May 2025, Scheduled 23 May 2025)

Optimization of MIMO Radar Sparse Array Based on Improved Adaptive Genetic Algorithm

Shun He[1], Junting Wang[1,*], and Zhiwei Yang[2]

[1] College of Communication and Information Engineering, Xi'an University of Science and Technology, Xi'an 710054, China
[2] College of Electronic Engineering, Xidian University, Xi'an 710126, China

ABSTRACT: In order to solve the problem of transceiver array optimization for multiple input multiple output (MIMO) radar under the conditions of fixed number of array elements and aperture length, an improved adaptive genetic algorithm is proposed in this paper. The algorithm takes the joint transceiver beam of MIMO radar as the optimization target and optimizes the positions of the array elements of the transmitting and receiving arrays by introducing new crossover and mutation operators and elite protection strategies, which effectively reduces the number of array elements, while maintaining the mainlobe gain and reducing the sidelobe level. The effectiveness and superior optimization performance of the proposed algorithm are verified through experiments, which has certain theoretical reference significance in MIMO radar design.

1. INTRODUCTION

In the field of modern radar, MIMO radar [1–5], as an innovative radar architecture, has attracted much attention and in-depth research from academics by virtue of its outstanding performance in key performance indicators such as target detection, target identification, and parameter estimation [6–8]. MIMO radar realizes high-resolution detection of targets by transmitting orthogonal signals between transmitting arrays and adopting matched filtering and beam formation at the receiving end. The system not only improves the radar's spatial performance, but also improves the radar's performance. This system not only improves the spatial resolution of the radar, but also enhances its anti-jamming capability in complex environments.

In practice, however, the performance of a MIMO radar depends heavily on the design of the array structure [9], and the configuration of the array directly affects the angular resolution. MIMO array design [10–13] is required to make the virtual array aperture large and to guarantee the performance. A large virtual array aperture usually requires the virtual array to be sparse, so both the transmitting and receiving arrays need to be sparse [14]. Optimizing the positions of array elements in a MIMO array, especially when it is subject to constraints like minimum array-element spacing and physical aperture size, is a nonlinear and highly multi-peaked problem. Conventional optimization techniques struggle to solve this problem efficiently. In recent years, scholars have proposed to use intelligent optimization algorithms to solve this problem, including genetic algorithm (GA) [15], simulated annealing algorithm [16], particle swarm algorithm [17], and ant lion optimizer (ALO). As an efficient, practical, and robust optimization method, the genetic algorithm exhibits unique advantages in searching for global optimal solutions. Unlike other optimization methods, it requires no initial information to perform optimization, ensuring wide applicability. Srinivas and Patnaik [18] proposed an adaptive genetic algorithm (AGA) based on GA. The core of AGA is replacing fixed mutation and crossover probabilities with a dynamic adjustment mechanism. However, this method fails to significantly reduce the algorithm's likelihood of falling into local optima. Ref. [19] improved the AGA and named it adaptive genetic algorithm-1 (AGA-1) in this paper. The algorithm dynamically adjusts mutation and crossover probabilities based on individual fitness to optimize the search process. However, due to a high mutation probability in the late evolutionary stage, it converges slowly. Ref. [20] improved the GA mutation operator and named it adaptive genetic algorithm-2 (AGA-2) in this paper. The algorithm gradually increases the mutation probability in the late evolutionary stage, effectively mitigating the issue of local convergence. However, it overlooks two key aspects: population fitness changes during each evolution and whether newly generated individuals exhibit improved fitness. Ref. [21] proposed a sparse array optimization method based on AGA. It takes the maximum array aperture, minimum array element spacing, and the lower bound of the Cramér-Rao bound as constraints. This enables it to better adapt to populations of different generations and accelerate the convergence speed. However, the algorithm is prone to getting trapped in local optima. Ref. [22] proposed a new multi-objective quantum genetic algorithm. This algorithm combines the advantages of the quantum genetic algorithm and non-dominated sorting genetic algorithm, enhancing the algorithm's global search ability and population diversity. However, the performance of the algorithm may be affected by parameters such as the population size and the maximum number of iterations, which makes it difficult for the algorithm to find the optimal solution. Ref. [23] proposed a sparse array optimization method. It combines an

* Corresponding author: Junting Wang (wangjunting@stu.xust.edu.cn).

improved genetic algorithm with Gaussian process regression to optimize antenna positions and reduce the sidelobe level. However, during the evolutionary process, it is still prone to getting trapped in local optima.

To address the issue that existing algorithms tend to prematurely converge to local optima during MIMO radar sparse antenna array optimization, this paper proposes an improved AGA. This algorithm is applied to the joint optimization of MIMO radar's transmitting and receiving arrays. By simultaneously optimizing the positions of transmitting and receiving array elements with this algorithm, we can achieve lower peak sidelobes while reducing the number of array elements. This enhances the performance of MIMO radar.

2. MIMO RADAR SPARSE ARRAY MODEL

The MIMO radar system in this paper is set in a single-base configuration and operates in the far-field region, where the azimuthal angles of the detected targets with respect to the transmitting and receiving arrays are spatially consistent. The transmitting array of the radar system is set to contain M array elements, and the receiving array contains N array elements, as shown in Fig. 1.

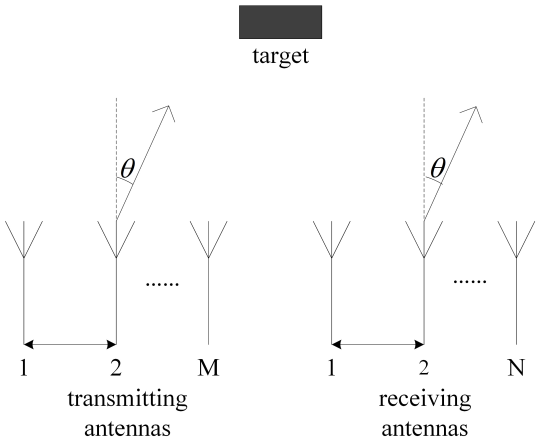

FIGURE 1. MIMO radar schematic.

The positions of the transmitting array elements are:

$$d_t = [d_{t,0}, d_{t,1}, d_{t,M-1}] \tag{1}$$

The positions of the receiving array elements are:

$$d_{\mathrm{r}} = [d_{r,0}, d_{r,1}, d_{r,N-1}] \tag{2}$$

where $d_{t,m}$ and $d_{r,n}$ denote the position of the mth transmitting array element and the position of the nth receiving array element, $m = (0, 1, 2, \cdots, M-1)$,$n = (0, 1, 2, \cdots, N-1)$.

It is known from [16] that the equivalent transmitting and receiving direction map of the MIMO radar can be expressed as:

$$F(u) = \left| \sum_{m=0}^{M-1} w_{t,m}^{*} \cdot e^{(j2\pi d_{t,m} \cdot u)/\lambda} \right| \times \left| \sum_{n=0}^{N-1} w_{r,n}^{*} \cdot e^{(j2\pi d_{r,n} \cdot u)/\lambda} \right| \tag{3}$$

where w_t and w_r correspond to the weighting coefficients of the virtual transmitter and receiver beam formation; $u = \sin\theta - \sin\theta_0$, respectively; θ is the scanning direction; and θ_0 is the viewing direction. For any $\theta, \theta_0 \in [-\pi, \pi]$, $u \in [-2, 2]$, $w_t = s_t$, $w_r = s_r$. s_t and s_r are the guidance vectors of the transmitting and receiving arrays, respectively, and the mathematical expressions of the two can be specifically defined as:

$$s_t = [1, e^{(-j2\pi d_{t,1} \sin\theta)/\lambda}, \cdots, e^{(-j2\pi d_{t,M-1} \sin\theta)/\lambda}]^{\mathrm{T}} \tag{4}$$

$$s_r = [1, e^{(-j2\pi d_{r,1} \sin\theta)/\lambda}, \cdots, e^{(-j2\pi d_{r,N-1} \sin\theta)/\lambda}]^{\mathrm{T}} \tag{5}$$

After normalization, the direction map function can be expressed as:

$$F(u) = 20\lg\left(\frac{F(u)}{\max(F(u))}\right) \tag{6}$$

The main objective of MIMO radar sparse array optimization is to suppress the sidelobe level of the antenna array direction map. Therefore, in this paper, the peak sidelobe level of the antenna array direction map is taken as the optimization objective function [24]. It represents the relative strength of the maximum sidelobe level based on the peak level of the mainlobe. Its mathematical expression is:

$$f(d_t, d_r) = \min\left\{\max_{\varphi \in S}\left\{20\lg\left(\frac{F(u)}{\max(F(u))}\right)\right\}\right\} \tag{7}$$

In the formula, "min" indicates the minimization function. $S = \{\theta \mid \theta_{\min} \le \theta \le \theta_0 - \theta_m \cup \theta_0 + \theta_m \le \theta \le \theta_{\max}\}$ is the sidelobe interval of the antenna array direction map. The beam scanning angle range is $[\theta_{\min}, \theta_{\max}]$, and the zero-power point of the mainlobe of the direction map is $2\theta_m$. The smaller the value of peak sidelobe level is [25], the greater the difference between the sidelobe level and mainlobe level is, and the stronger the radar's beam-forming capability is.

3. MIMO RADAR ARRAY OPTIMIZATION BASED ON IMPROVED AGA ALGORITHM

Aiming at the problems of AGA, an improved algorithm is proposed while retaining its advantages. A new crossover-mutation operator and an elite protection strategy are introduced. The improved algorithm comprehensively considers the influence of the number of iterations on the population's evolutionary process and the change in the population's adaptability in each generation. It also adopts a nonlinear adjustment strategy to dynamically adjust the crossover probability and mutation probability. Meanwhile, this paper applies the improved algorithm to the optimization problem of the MIMO radar array. The optimization model is shown in Eq. (7). The operation steps of the improved algorithm are as follows.

3.1. Initializing the Population

In this paper, a binary coding approach is used. Specifically, the array parameters are characterized by binary digitization. According to the modeling framework of mathematical expressions in Eqs. (1) and (2), the genetic coding sequences of the transmitter-side and receiver-side, namely the transmitter-side coding sequence and receiver-side coding sequence, are constructed respectively. In this coding system, each binary bit

corresponds to a discretized grid position. Here, "1" indicates the presence of a valid array element at the grid point, while "0" indicates that the array element is vacant. To meet the constant-aperture constraint and ensure array elements at the start and end grids of both transmitting and receiving arrays, the following constraints are defined for the coding scheme:

$$\text{cheom}_t = \{1, 0, 1, \cdots, 1\} \tag{8}$$

$$\text{cheom}_r = \{1, 1, 0, \cdots, 1\} \tag{9}$$

The population size is set to NP, and the maximum number of evolutions is set to G. Repeat the above process NP times to complete the population initialization.

3.2. Fitness Function

The fitness function is the basis for the genetic algorithm's selection operation. It is also closely related to the algorithm's iteration termination conditions and problem constraints. To reduce the number of array elements and lower the peak sidelobe level of the antenna array directional map, this paper adopts Eq. (7) as the fitness function. Using this fitness evaluation function, calculate the fitness value of each individual in the current population and sort them in ascending order. Then, check if the termination condition is met. If yes, output the optimal individual as the optimization result. If not, proceed to the next iteration. In this paper, the termination condition is set as reaching the maximum number of iterations.

3.3. Choice Operators and Elite Protection Strategies

In this paper, we adopt a probabilistic selection mechanism based on fitness proportion and integrate an elite protection strategy to construct the selection operator. The elite protection strategy inherits contemporary optimal individuals to the next-generation population without perturbation. This effectively avoids the loss of high-quality solutions caused by the disturbance of genetic operations. This strategy ensures the integrity of the optimal solution during population evolution. Meanwhile, by reducing the probability of random destruction of high-quality genes, it significantly improves the algorithm's convergence efficiency and the stability of the optimization process. Specifically, the number of elite individuals is first determined according to a preset elite proportion (2% in this paper). That is, the top 2% of individuals in the population are retained. In each generation, current optimal individuals are selected by calculating their fitness values and copied to the next generation.

3.4. Improved Crossover and Mutation Operators

The traditional AGA dynamically adjusts the fixed crossover and variance probabilities by the following equation [18]:

$$P_c = \begin{cases} k_1(f_{\max} - f')/(f_{\max} - f_{\text{avg}}), & f' \geq f_{\text{avg}} \\ k_3, & f' < f_{\text{avg}} \end{cases} \tag{10}$$

$$P_m = \begin{cases} k_2(f_{\max} - f)/(f_{\max} - f_{\text{avg}}), & f \geq f_{\text{avg}} \\ k_4, & f < f_{\text{avg}} \end{cases} \tag{11}$$

where $f_{\max}$ denotes the fitness value of the optimal individual in the population, f_{avg} the mean value of the overall fitness level of the population, f' the higher fitness value of the parent individual involved in the crossover, f the fitness value of the variant individual, and $0 < k_1, k_2, k_3, k_4 \leq 1$.

Compared with the traditional GA, the adjusted algorithm dynamically adjusts crossover and mutation probabilities based on individual fitness. For individuals with fitness lower than the population mean, the algorithm maintains higher crossover and mutation probabilities. On the contrary, when individual fitness exceeds the population mean, these probabilities decay exponentially with increasing fitness and eventually approach zero. This regulatory mechanism stabilizes the genetic structure of high-quality individuals, significantly accelerating the algorithm's convergence. However, it may induce immature convergence. When the population's optimal individuals are in a local extreme state, the algorithm terminates global search prematurely. This leads to insufficient exploration of the solution space, a phenomenon particularly evident when the initial population distribution deviates from the global optimal region.

In order to solve this problem, this paper improves the crossover probability and variation probability [18, 19, 23], and the improved formulas are denoted as:

$$P_c(i) = P_{c0} \cdot (1 - F_i) \tag{12}$$

$$P_m = P_{m0} - (P_{m0} - P_{m1}) \cdot \frac{k}{G} \tag{13}$$

where P_{c0} is the global crossover rate, used to control the overall frequency of crossover operations; F_i is the normalized fitness value of the ith individual, with a value in the range of $[0, 1]$; P_{m0} and P_{m1} are fixed parameters; and k denotes the current number of iterations. With this improved strategy, the algorithm can maintain the appropriate search capability while ensuring the stability of high fitness individuals, which helps to find the global optimal solution beyond the local optimization.

Equations (12) and (13) consider both individual fitness and population evolutionary generations, thus realizing adaptive regulation of crossover probability and variation probability. The core ideas of the algorithm include:

(a) Adaptation-based crossover probability: This strategy dynamically adjusts crossover probabilities, allowing higher-fitness individuals to have greater retention likelihood while assigning increased crossover probability to lower-fitness individuals. This approach enhances population diversity while protecting superior genetic material.

(b) Dynamically adjusting the mutation rate: as the number of iterations increases, the mutation rate gradually decreases. A higher variance rate at the initial stage helps to expand the search space and increase population diversity, while a lower variance rate at the later stage helps to improve the stability and convergence accuracy of the algorithm.

In addition, to ensure that the sparsity of each individual in the newly generated population remains unchanged after the crossover and mutation operations, i.e., the number of 0 s and 1 s in the individuals is maintained constant, it is ensured that the transceiver array contains M and N arrays, respectively, and that arrays are present at both transceiver and transmitting ends.

When a predetermined number of iterations is reached, the algorithm terminates and outputs the optimal individual as the final optimization result. The flowchart of the improved AGA algorithm in this paper is shown in Fig. 2.

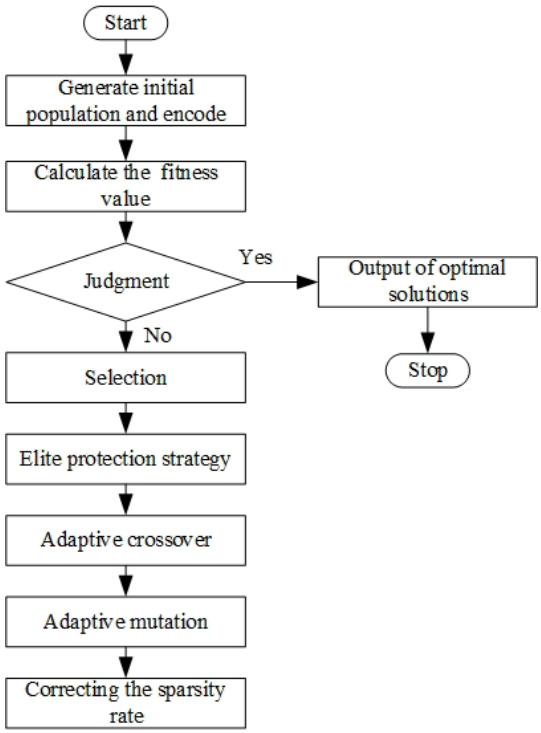

FIGURE 2. Flowchart of the algorithm proposed in this paper.

4. SIMULATION EXPERIMENTS AND RESULT ANALYSIS

In order to verify the performance of the proposed algorithm in this paper, it is compared and analyzed with GA, AGA, AGA-1, AGA-2, and ALO algorithm [26] in this section. To ensure the fairness of the comparison results, the experiment uniformly sets the population size to 200, the maximum number of iterations to 200, and uses Eq. (7) as the optimization objective function. The specific parameter settings of each algorithm are shown in Table 1.

TABLE 1. Parameter settings of the algorithms.

Algorith	Parameter setting
GA	$P_c = 0.8, P_m = 0.1$
AGA	$k_1 = k_2 = k_3 = 0.5, k_4 = 0.8$
AGA-1	$P_{c2} = 0.8, P_{m2} = 0.01, \phi = 0.18, \varphi = 0.9$
AGA-2	$P_c = 0.8, P_{m0} = 0.1$
ALO	$NP = 200, G = 200$
Our	$P_{m0} = 0.05, P_{m1} = 0.01, P_{c0} = 0.8$

In this paper, the numbers of transmitting and receiving array elements are set to 15, 25, and 35, respectively. These elements are arranged on a grid of integer multiples of the half-wavelength within the range $0 \sim 50\lambda$. The mainlobe pointing direction is set to $0°$. The entire aperture range is divided into 101 grid points. To maintain a constant maximum array aperture, one array element is fixed on each of the 1st and 101st grid points, while the remaining elements are randomly distributed across the other grid points.

Under different numbers of array elements and the same array aperture, the proposed algorithm is compared with GA, AGA, AGA-1, AGA-2, and ALO. A total of 100 independent random experiments are conducted, and the optimization results are shown in Table 2. The mean, minimum, maximum, and variance of the fitness function are recorded in detail. Analysis of the data shows that the proposed algorithm outperforms the other algorithms. This indicates that our algorithm has superior performance. It can solve the global optimal solution more accurately and has a stronger search capability. In addition, the variance of the optimized value is relatively small. This shows that the algorithm can maintain high stability during the convergence process, ensuring the reliability of the optimization results.

Comparison of the optimized directional patterns and convergence curves for the algorithms is shown in Figs. 3 and 4 when the number of array elements is 25, and the maximum number of iterations is 200. In Fig. 3 the green, cyan, blue, black, magenta, and red curves correspond to the GA, AGA, AGA-1, AGA-2, ALO, and the joint transceiver directional maps optimized by the improved algorithm proposed in this paper, respectively. Fig. 3(b) is a partially enlarged view of the black dashed line box in Fig. 3(a).

As can be seen from Fig. 3(a), the optimized joint transceiver direction map obtained by the improved algorithm proposed in this paper, as well as the rest of the algorithms, all have narrower mainlobe widths, which indicates that they all have better angular resolution capabilities. However, the peak sidelobe level corresponding to the improved algorithm in this paper is lower than the other five algorithms. This can be clearly seen in Fig. 3(b), which shows that the improved algorithm can optimize the peak sidelobe level to -26.8135 dB, while the peak sidelobe levels of the GA, AGA, AGA-1, AGA-2, and ALO are -25.1444 dB, -25.2899 dB, -25.2429 dB, -25.53 dB, and -22.8356 dB. It can be seen that this paper's algorithm has the lowest peak sidelobe level, indicating that its solution accuracy is higher than the other five algorithms, and the optimization effect is better.

Figure 4 shows the change curves of each algorithm's fitness with the number of iterations. The algorithm proposed in this paper is always below the rest of the algorithms in the fitness value change curve during the whole iteration process. This shows that compared with the other algorithms, the proposed algorithm is more efficient, has a stronger ability to jump out of the local optimum, and performs better. Moreover, the fitness curve of this paper's algorithm decreases faster in the 1st–50th iterations. This indicates that it has a higher search speed for the optimal solution. It also has a stronger ability to jump out of the local optimal solution after the convergence stagnation. Besides, it has a higher probability of producing offspring with better fitness values and can search the solution space more targeted.

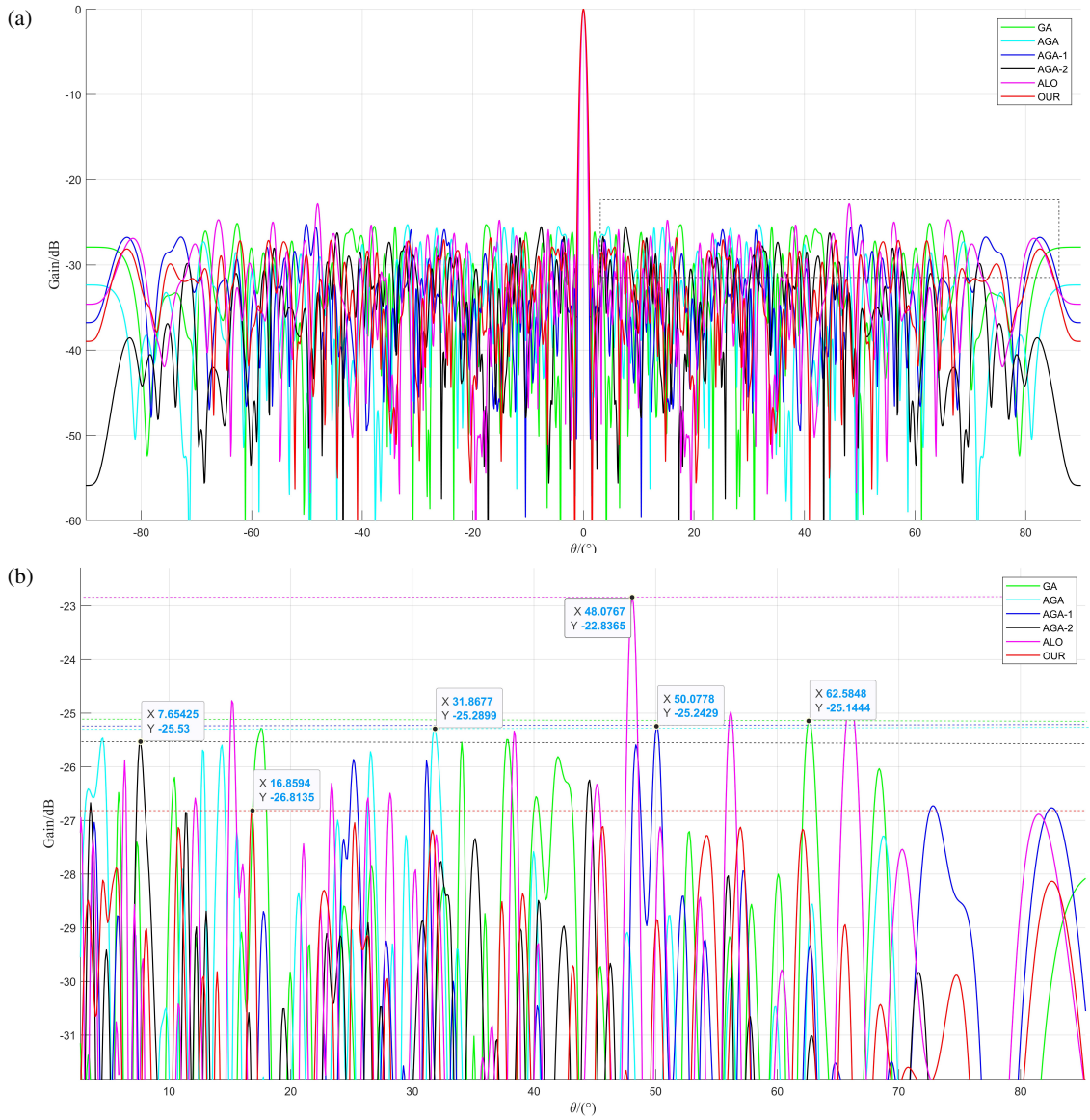

FIGURE 3. Optimized equivalent joint transceiver direction diagram. (a) Global results chart. (b) Localized results map.

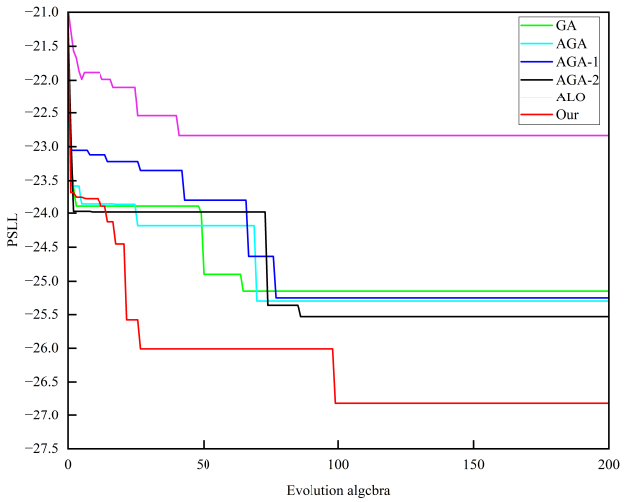

FIGURE 4. Variation curve of fitness of each algorithm with the number of iterations.

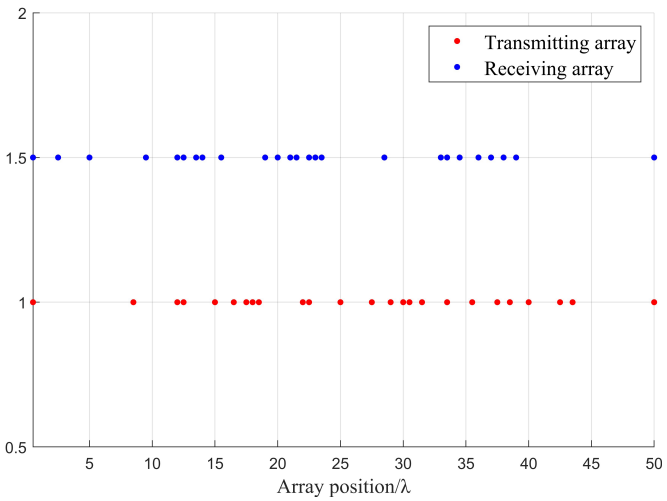

FIGURE 5. Location map of transceiver array elements solved by the improved method.

TABLE 2. Comparison of optimization results.

algorithm	mean/dB	min/dB	max/dB	std	mean/dB	min/dB	max/dB	std	mean/dB	min/dB	max/dB	std
	$M = N = 15$				$M = N = 25$				$M = N = 35$			
GA	−18.695	−19.151	−18.217	0.065	−24.384	−25.144	−23.721	0.076	−28.745	−29.212	−28.192	0.091
AGA	−19.079	−19.427	−18.428	0.057	−24.562	−25.289	−24.059	0.069	−28.483	−29.145	−28.214	0.077
AGA−1	−18.492	−19.616	−17.787	0.159	−24.349	−25.242	−23.435	0.279	−28.078	−29.138	−27.293	0.177
AGA−2	−18.778	−19.369	−18.176	0.072	−24.353	−25.530	−23.857	0.079	−28.659	−29.696	−28.144	0.078
ALO	−15.368	−16.823	−14.138	1.713	−21.380	−22.836	−19.448	1.591	−25.692	−27.034	−24.006	1.637
Our	−19.331	−20.423	−18.541	0.158	−25.421	−26.813	−24.575	0.246	−29.878	−31.084	−28.832	0.234

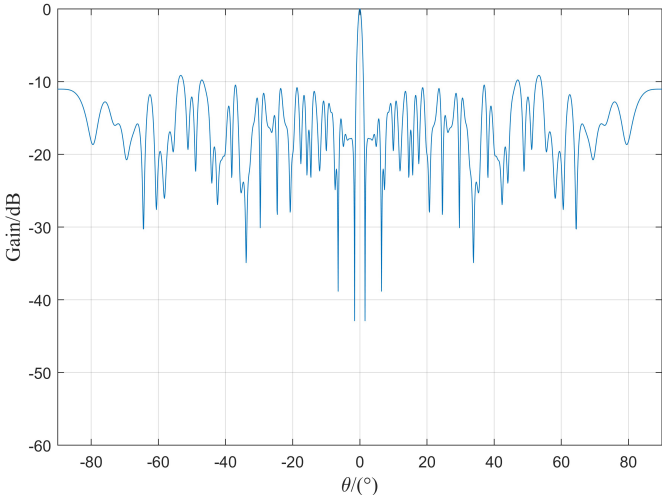

FIGURE 6. Equivalent emission direction diagram.

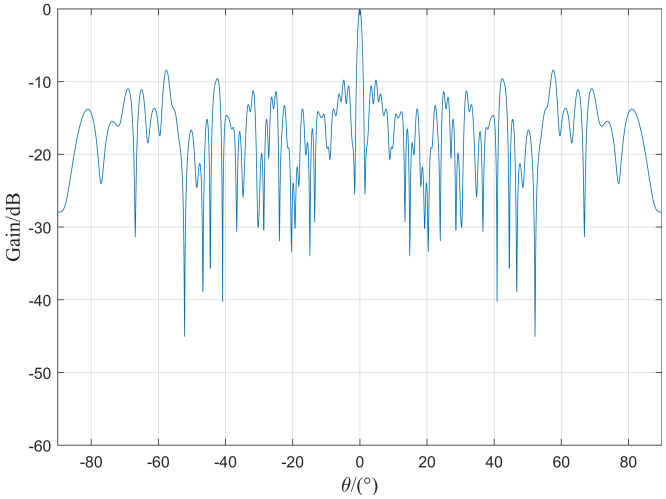

FIGURE 7. Receive direction chart.

TABLE 3. The performance of the M = N = 25 array under the same aperture.

Algorith	peak sidelobe level
literature [26]	−25.8809 dB
This article method	−26.8135 dB

Figure 5 shows the positional distribution of the transmitting and receiving array array elements for the optimized 25 array elements. The optimized transmitting array element positions are [0 8 11.5 12 14.5 16 17 17.5 18 21.5 22 24.5 27 28.5 29.5 30 31 33 35 37 38 39.5 42 43 50] $\times\lambda$, and the receiving array element positions are [0 2 4.5 9 11.5 12 13 13.5 15 18.5 19.5 20.5 21 22 22.5 23 28 32.5 33 34 35.5 36.5 37.5 38.5 50] $\times\lambda$.

Based on the array element positions determined by the proposed algorithm, the equivalent transmitting-receiving direction maps of the MIMO radar can be obtained. The specific results are shown in Fig. 6 and Fig. 7. Fig. 6 shows the equivalent transmitting direction map, and Fig. 7 shows the receiving direction map. From the figures, it can be clearly seen that the performance of the equivalent transmitting direction map and receiving direction map is poor, with high sidelobe levels. Therefore, to improve the radar's overall performance significantly, joint optimization of the transmitting and receiving arrays is crucial. This can effectively suppress the sidelobe and enhance the effectiveness of target detection.

Table 3 shows the performance comparison of the peak sidelobe level for the array with $M = N = 25$ under the same aperture. Compared with the method in [26], the sidelobe-suppression performance of the method in this paper is superior. It can more effectively reduce the sidelobe level and enhance the array performance.

5. CONCLUSION

In this paper, an improved adaptive genetic algorithm (AGA) is proposed for MIMO radar array optimization. We introduce new crossover and mutation operators and incorporate an elite protection strategy. The transmitting and receiving arrays are non-uniformly distributed linear arrays. Trials show that, under fixed array aperture and element count, the proposed method effectively suppresses sidelobes while maintaining mainlobe width. Compared with other optimization algorithms, it achieves faster convergence. In addition, there is a difference between single-base and dual-base MIMO radars. After matched filtering, the starting points of their equivalent phase centers are different, but the phase relationships between the equivalent phase centers of each matched filtering output are the same. The method in this paper is based on the equivalent transceiver directional map for optimization. Thus, it can be used for sparse array optimization of dual-base MIMO radars. In other words, it can be extended to other MIMO array

optimization. This has certain reference value for the optimal design and engineering application of array antennas.

ACKNOWLEDGEMENT

The authors would like to thank the editors and anonymous reviewers for their efforts in evaluating our manuscript.

This work was supported in part by the National Natural Science Foundation of China, Grant 62271386.

REFERENCES

[1] Kalkan, Y., "20 years of MIMO radar," *IEEE Aerospace and Electronic Systems Magazine*, Vol. 39, No. 3, 28–35, 2024.

[2] Yu, X., X. Yao, J. Yang, L. Zhang, L. Kong, and G. Cui, "Integrated waveform design for MIMO radar and communication via spatio-spectral modulation," *IEEE Transactions on Signal Processing*, Vol. 70, 2293–2305, 2022.

[3] Wang, X., W. Zhai, X. Zhang, X. Wang, and M. G. Amin, "Enhanced automotive sensing assisted by joint communication and cognitive sparse MIMO radar," *IEEE Transactions on Aerospace and Electronic Systems*, Vol. 59, No. 5, 4782–4799, 2023.

[4] Buzzi, S., E. Grossi, M. Lops, and L. Venturino, "Foundations of MIMO radar detection aided by reconfigurable intelligent surfaces," *IEEE Transactions on Signal Processing*, Vol. 70, 1749–1763, 2022.

[5] Niu, B., Y. Zhao, and D. Tang, "Waveform agile MIMO radar fast waveform design based on random arrangement of pulse slices," *Signal Processing*, Vol. 230, 109784, 2025.

[6] Tang, W.-G., H. Jiang, Q. Zhang, and H. Jiang, "PSWF-based decoupled atomic norm minimization for DOD and DOA estimation in MIMO radar with arbitrary linear arrays," *Signal Processing*, Vol. 212, 109136, 2023.

[7] Liu, Y., X. Zhang, and Q. Yang, "DOA estimation of multiple coherent targets using weight vector orthogonal decomposition in TDM-MIMO HF-radar," *Remote Sensing*, Vol. 15, No. 16, 4073, 2023.

[8] Wen, F., J. Shi, G. Gui, C. Yuen, H. Sari, and F. Adachi, "Joint DOD and DOA estimation for NLOS target using IRS-aided bistatic MIMO radar," *IEEE Transactions on Vehicular Technology*, Vol. 73, No. 10, 15 798–15 802, 2024.

[9] Bui, L. T. P., N. Anselmi, G. M. Battaglia, T. Isernia, P. Rocca, and A. F. Morabito, "Synthesis of wideband reconfigurable array antennas for monopulse radar applications," *Progress In Electromagnetics Research M*, Vol. 106, 179–189, 2021.

[10] Ma, Y., C. Miao, Y. Zhao, and W. Wu, "An MIMO radar system based on the sparse-array and its frequency migration calibration method," *Sensors*, Vol. 19, No. 16, 3580, 2019.

[11] Liang, C., Y. Wang, Z. Yang, X. Hu, Q. Pei, W. Gu, and L. Zhang, "Cooperative automotive radars with multi-aperture multiplexing MIMO sparse array design," *Electronics*, Vol. 11, No. 8, 1198, 2022.

[12] Sayin, A., E. G. Hoare, and M. Antoniou, "Design and verification of reduced redundancy ultrasonic MIMO arrays using simulated annealing & genetic algorithms," *IEEE Sensors Journal*, Vol. 20, No. 9, 4968–4975, 2020.

[13] Wang, X.-K., G.-B. Wang, and L. Wang, "Pattern synthesis for different sparse planar arrays by a hybrid unconstrained-heuristic approach," *IEEE Antennas and Wireless Propagation Letters*, Vol. 22, No. 3, 631–635, 2022.

[14] Battaglia, G. M., T. Isernia, R. Palmeri, and A. F. Morabito, "Four-beams-reconfigurable circular-ring array antennas for monopulse radar applications," *Radio Science*, Vol. 58, No. 9, 1–14, 2023.

[15] Huang, Y., L. Ma, X. Yu, H. Zhang, J. Li, and X. Xi, "MIMO antenna array design based on genetic algorithm," in *2021 IEEE 4th International Conference on Electronic Information and Communication Technology (ICEICT)*, 406–409, Xi'an, China, Aug. 2021.

[16] Zhang, W., Z.-S. He, and J. Li, "Optimization design of MIMO radar sparse array," *Systems Engineering and Electronics*, Vol. 35, No. 2, 299–303, 2013.

[17] Feng, C., H. Ye, H. Hong, E. Wang, and X. Zhu, "A hybrid algorithm for sparse antenna array optimization of MIMO radar," in *2022 IEEE Radio and Wireless Symposium (RWS)*, 115–117, Las Vegas, NV, USA, Jan. 2022.

[18] Srinivas, M. and L. M. Patnaik, "Adaptive probabilities of crossover and mutation in genetic algorithms," *IEEE Transactions on Systems, Man, and Cybernetics*, Vol. 24, No. 4, 656–667, 1994.

[19] Liang, H., X. B. Li, and X. Y. Xu, "Array optimization for MIMO radar based on improved adaptive genetic algorithm," *J. Microw.*, Vol. 29, No. 4, 12–19, 2013.

[20] Li, L., J. Wang, G. Wu, and W. Long, "Optimization of sparse array based on adaptive genetic algorithm," *Modern Radar*, Vol. 39, No. 03, 59–61, 2017.

[21] Chen, T., X. Wang, L. Shi, and M. Shen, "Array sparse optimization method based on adaptive genetic algorithm," in *IET Conference Proceedings CP779*, Vol. 2020, No. 9, 1271–1275, 2020.

[22] Liu, T., J. Sun, G. Wang, and Y. Lu, "A multi-objective quantum genetic algorithm for MIMO radar waveform design," *Remote Sensing*, Vol. 14, No. 10, 2387, 2022.

[23] Yang, H., P. Chen, H. Zhou, and J. Tan, "An efficient position optimization method based on improved genetic algorithm and machine learning for sparse array," *AEU — International Journal of Electronics and Communications*, Vol. 179, 155312, 2024.

[24] Battaglia, G. M., G. G. Bellizzi, A. F. Morabito, G. Sorbello, and T. Isernia, "A general effective approach to the synthesis of shaped beams for arbitrary fixed-geometry arrays," *Journal of Electromagnetic Waves and Applications*, Vol. 33, No. 18, 2404–2422, 2019.

[25] Battaglia, G. M., A. F. Morabito, G. Sorbello, and T. Isernia, "Mask-constrained power synthesis of large and arbitrary arraysas a few-samples global optimization," *Progress In Electromagnetics Research C*, Vol. 98, 69–81, 2020.

[26] Lu, J.-S., Z.-K. Zhang, *et al.*, "Optimized design of MIMO radar array pattern based on ant lion optimizer," *Electronics Optics & Control*, Vol. 28, No. 4, 77–81, 2021.